Constraint Release in Moderately Entangled Monodisperse Star Polyisoprene Systems

Xiuying Qiao,[†,‡] Toshiaki Sawada,[†] Yumi Matsumiya,[†] and Hiroshi Watanabe*,[†]

Institute for Chemical Research, Kyoto University, Uji, Kyoto 611-0011, Japan, and State Key Laboratory of Metal Matrix Composites, Shanghai Jiao Tong University, Shanghai, 200030, P. R. China

ABSTRACT: For examination of a constraint release (CR) contribution to relaxation in monodisperse systems of moderately entangled six-arm star polyisoprenes (PI), viscoelastic measurements were conducted for blends of these star PI and a high molecular weight (M) linear PI. In the blends, the linear PI was dilute and entangled only with the matrix star chains. The terminal relaxation of this dilute linear probe occurred through competition of reptation and Rouse-type CR, as confirmed from its relaxation mode distribution. The probe relaxation time τ_{probe} measured in the blends was utilized in the following way to elucidate the CR relaxation in the star matrices: Since the CR time τ^{CR} of the star matrix is expressed as $(2N_a)^2 \tau_{life}$ with $2N_a$ and τ_{life} being the entanglement number per two arms (span length) and the effective entanglement lifetime in the system, τ^{CR} can be evaluated if the τ_{life} value is known. For determination of the τ_{life} value, the τ_{probe} data of the linear probe in the star matrices was compared with the previously obtained τ_{probe} data of the *same* probe in linear PI matrices under a molecular idea that τ_{life} should be the same in a *pair* of star and linear matrices giving the same τ_{probe} value. The molecular weight $M_{L,mat}$ of the linear matrix paired with each star matrix was thus specified, and the value of τ_{life} in the star matrix was determined by utilizing this $M_{L,mat}$ value in a previously obtained empirical equation of τ_{life} in the linear matrices ($\tau_{life} = 2.5 \times 10^{-18} M_{L,mat}^3$ s at 40 °C). For the monodisperse systems of the star PI, the τ^{CR} ($= (2N_a)^2 \tau_{life}$) thus evaluated was close to the measured relaxation time, indicating that the CR mechanism significantly contributes to the star relaxation. This result was in harmony with the validity of the molecular picture of partial dynamic-tube-dilation (p-DTD) confirmed for the star PI.

1. Introduction

As an interdisciplinary research field, the entanglement dynamics of flexible polymers has been attracting wide research interest of physicists and chemists for long time, thus promoting the continual development of the theoretical framework of the tube model.[1−4] Extensive experiments indicate that the molecular weight, molecular weight distribution, and the chain architecture have significant effects on dynamic properties of polymers,[1−4] and the tube model has been refined so as to explain all these effects. For the research of rheology and molecular dynamics of entangled polymers, the linear and star-branched polymers compose the major database due to the simplicity of their structures, although recent research has been also extended to the polymers with more complicated structures such as the pom-poms[5,6] and hyperbranched[7,8] polymers.

Binary blends of monodisperse linear and/or star chains are the best model systems for investigation of the relaxation mechanisms related to the lifetime of the entanglement.[3,4,9−15] In particular, if one component in the blend is dilute and entangled only with the other component, the entanglement lifetime for the dilute component (probe) is easily tuned through the molecular weight/topological architecture of the major component (matrix). For such dilute probe chains entangled with much shorter matrix chains, the constraint release[1−4] (CR) relaxation activated by the matrix motion has been clearly detected from viscoelastic experiments[9,10,16−19] and its detailed

features (delicate non-Rouse features reflected in the CR eigenfunctions[3,20,21]) have been discussed. Furthermore, for the molecular picture of dynamic tube dilation (DTD)[3,4] incorporated in the current tube model(s), recent experiments[18,22,23] indicated that the CR process plays an important role in the self-consistent determination of the dilated tube diameter and that the molecular picture of partial-DTD based on this self-consistency is valid for linear and star chains.

Because of this importance of the CR mechanism for the entanglement relaxation, it is strongly desired to experimentally characterize the CR features (relaxation time and mode distribution) for representative polymer systems. For polystyrene (PS), the CR relaxation of *dilute* probes was investigated rather extensively[3,9,10,16,17] (for linear/star probes in linear/star matrices). In contrast, for *cis*-polyisoprene (PI) utilized in the test of the DTD picture, the CR relaxation of dilute linear probes in linear matrices was fully characterized recently,[19] but only limited data have been obtained for star probes: The data are available just for high molecular weight (M) star probes having the arm entanglement number $N_a = M_a/M_e \geq 12$.[18] Thus, it was desired to characterize the CR behavior also for star PI with lower N_a so that the partial DTD picture can be tested for star PI systems in a wider range of N_a.

The standard method of characterizing the pure CR process, the viscoelastic measurement for blends of dilute probes in *much shorter* matrix chains,[9,16−19] cannot apply to the lower-N_a star PI probe explained above because the matrix chains much shorter than this probe are no longer in the entangled regime. Thus, following a previous strategy[10] for this characterization, we examined the viscoelastic behavior of dilute high-M linear PI probe in low-N_a star PI matrices: Considering the equivalence

* To whom correspondence should be addressed. E-mail: hiroshi@scl.kyoto-u.ac.jp.
† Institute for Chemical Research, Kyoto University.
‡ State Key Laboratory of Metal Matrix Composites, Shanghai Jiao Tong University.

of the effects of the star and linear matrices on the probe relaxation,[10] we compared the relaxation time of the same probe in linear and star matrices to evaluate the CR time for the star matrices themselves. Furthermore, we utilized the CR time thus obtained for the moderately entangled star PI to examine the validity of the partial DTD picture for these star PI. The results are presented in this paper. First, in section 2, the method of the evaluation of the CR time for the low-N_a star matrices is explained. Section 3 summarizes the experimental conditions. Then, section 4 presents the experimental data, the analysis for evaluation of the CR time for those star PI, and the results of the test of partial-DTD picture for these star PI. Finally, a summary of this study is given in section 5.

2. Method of Evaluation of CR Time for Low-N_a Star Matrix

For star chains having a low-to-moderate number of entanglements per arm, $N_a < 10$, the pure CR process cannot be characterized with the standard method, the viscoelastic measurement for blends containing these star chains as the high-M dilute probes entangled with *much shorter* matrix chains, because such short matrix chains are no longer in the entangled regime. However, we can still determine the CR time of the low-N_a star chains with the previously utilized method.[10]

This method focuses on the relaxation of dilute high-M linear probe chains in matrices of shorter star and linear chains. The terminal relaxation of this linear probe occurs through competition of the CR process activated by the motion of the matrix chains and the reptation process of the probe itself[3,4,9,10,16,17,19] and thus the probe relaxation time τ_{probe} is determined according to the values of the CR and reptation times of the probe, τ_{probe}^{CR} and τ_{probe}^{rep}. Experiments[3,16,17,19] indicate that the terminal CR time of the linear probe is well described by the Rouse−CR relationship

$$\tau_{probe}^{CR} = N_{probe}{}^2 \tau_{life}(matrix) \quad (1)$$

Here, N_{probe} is the number of entanglements per linear probe ($N_{probe} = M_{probe}/M_e$), and $\tau_{life}(matrix)$ is the effective entanglement lifetime in a given matrix determined by the matrix structure, i.e., the entanglement number N_{mat} and topological architecture (=linear or star) of the matrix chain. (In eq 1 and hereafter, a numerical proportionality constant[2] is absorbed in τ_{life}.)

Considering eq 1, we can *formally* express the measured τ_{probe} as a function of N_{probe}, τ_{life}, and the reptation time τ_{probe}^{rep}, with τ_{probe}^{rep} being dependent only on N_{probe}:

$$\tau_{probe} = F\{N_{probe}{}^2 \tau_{life}(matrix), \tau_{probe}^{rep}(N_{probe})\} \quad (2)$$

The functional form of F in eq 2 could be derived from a model-(s)[3,4] but this form is not required in our analysis. The essential point of eq 2 is that τ_{life} is the same in a pair of linear and star matrices if τ_{probe} of a linear given probe is the same in these two matrices.

We can consider this point to experimentally determine $\tau_{life}(star)$ in a focused star matrix, given that an empirical equation of $\tau_{probe}^{CR}(N_{probe}, N_{L,mat})$ of the linear probe in linear matrices is known as a function of the entanglement numbers N_{probe} and $N_{L,mat}$ of these probe and matrices. (This equation is indeed known for linear PI probes in linear PI matrices.[19]) For this determination, we first compare the τ_{probe} data of a given linear probe in the focused star matrix and in a series of linear matrices to specify a linear matrix in which τ_{probe} is the same

Table 1. Characteristics of PI Samples

sample	$10^{-3} M_w$	$10^{-3} M_a$	M_w/M_n
Six-Arm Star PI (Used as Matrix)			
6(I-09)	54.2	9.5	1.05
6(I-16)	95.4	16.0	1.03
6(I-24)	144	23.5	1.03
6(I-31)	181	30.6	1.04
6(I-41)	248	40.7	1.03
Linear PI (Used as Probe)			
L329	329		1.06

as that in the star matrix. Utilizing the entanglement number $N_{L,mat}*$ of this *equivalent* linear matrix in the empirical equation of τ_{probe}^{CR}, we can evaluate τ_{life} in the star matrix as $\tau_{life}(star) = \tau_{life}(linear) = N_{probe}{}^{-2}\tau_{probe}^{CR}(N_{probe}, N_{L,mat}*)$. For any star probe having N_a entanglement segments per arm, we can utilize this $\tau_{life}(star)$ value to determine the Rouse−Ham type terminal CR time[9] in the focused star matrix as

$$\tau_{star\ probe}^{CR} = \{2N_a\}^2 \tau_{life}(star) \quad (3)$$

The CR time in the monodisperse system of the focused star chains is obtained by utilizing the N_a value of these chains in eq 3.

We should note that the factor of $\{2N_a\}^2$ appears in eq 3 (instead of the factor of $N_{probe}{}^2$ in eq 1) because the slowest Rouse−Ham and/or tethered-Rouse CR eigenmode for the segment position of the star arm has a node at the branching point and is identical to the slowest mode for the linear probe of the length $2N_a$.[3] In other words, the span-length of the star probe corresponding to two arms is equivalent to the full length of the linear probe in the Rouse−Ham/tethered-Rouse CR dynamics, giving the molecular basis for the use of the factor of $\{2N_a\}^2$ in eq 3.

Here, it should be emphasized that the method explained above utilizes *neither* the model-dependent functional form of F (eq 2) describing the competition of reptation and CR *nor* the functional form (N_{probe} dependence) of τ_{probe}^{rep}. For this reason, the method is not limited to the CR-dominant case (for dilute probes in much shorter matrices). The method simply requires us to know an empirical equation of τ_{probe}^{CR} for the linear probe in linear matrices and to compare τ_{probe} data in star and linear matrices. Thus, this method provides us with the most reliable route of evaluating τ^{CR} for star chains with low-to-middle N_a values ($N_a = 2-8$ for star PI utilized in this study).

3. Experimental Section

3.1. Materials. Narrow molecular weight distribution (monodisperse) linear and six-arm star polyisoprene (PI) were utilized as the probe and matrices, respectively. These materials were anionically synthesized and characterized in the previous studies.[18,19,24−26] The linear PI sample, the dilute high-M probe in this study, was identical to the probe in the previous study of linear PI/linear PI blends,[19] and all star PI samples, the matrices in this study, were also utilized in the previous study of star PI/star PI blends.[18] These samples, containing a small amount (~0.05 wt %) of an antioxidant (butylhydroxytoluene), had been sealed in Ar atmosphere and stored in a deep freezer until use. Lack of chemical degradation during the storage was confirmed with GPC measurements.

Table 1 summarizes the characteristics of the star and linear PI samples (determined previously[18,19,24−26] from GPC combined with light scattering). The samples were coded as LX and 6(I−X) for linear and six-arm star PI, respectively, with the code-number X representing the molecular weight of the linear sample and/or star arm in unit of 1000. For all star samples, the arm had more than two entanglements; $N_a = M_a/M_e \geq 2$ with $M_e = \rho RT/G_N = 5.0 \times$

10^3 being the entanglement spacing for PI[27] evaluated from the gas constant R, PI density ρ ($\cong 0.92$ g cm^{-3}), and entanglement plateau modulus $G_N = 4.8 \times 10^5$ Pa at $T = 313$K (=40 °C). These star matrix chains were entangled with the high-M linear probe L329 ($N_{probe} = M/M_e = 66$).

The systems subjected to viscoelastic measurements were blends of L329 probe in matrices of six-arm star PI samples. The probe volume fraction v_{probe} was kept small ($v_{probe} \leq 0.01$) to ensure that the probe was dilute and entangled only with the star matrix. For preparation of these blends, prescribed masses of the linear and star samples were uniformly dissolved in benzene (at a total concentration $\cong 5$ wt %) and then benzene was allowed to thoroughly evaporate, first under atmospheric conditions and then in a high vacuum at 40 °C.

3.2. Measurement. For the linear/star PI blends, dynamic viscoelastic measurements were conducted with the Advanced Rheological Extending System (ARES, Rheometrics) in a parallel plate geometry (diameter = 25 mm) at temperatures between −30 and +80 °C. The oscillatory strain amplitude was kept small (≤ 0.05) to ensure the linearity of the viscoelastic response, and the storage and loss moduli, G' and G'', were recorded as a function of angular frequency ω in the range of 0.1−100 rad/s at each temperature. For some star samples, the dielectric responses were measured with an Impedance Analyzer 1260/Dielectric Interface 1296 (Solartron).

Prior to each run of the viscoelastic/dielectric measurements, the samples were annealed at respective temperatures for $\cong 10$ min to ensure stability/uniformity of the sample temperature. The time−temperature superposition worked for the viscoelastic and dielectric data, and all data were reduced/compared at a reference temperature $T_r = 40$ °C. The shift factor was well described by the previously reported empirical WLF equation,[22] log $a_T = -4.13(T - T_r)/(150 + T - T_r)$.

4. Results and Discussion

4.1. Overview of Probe Relaxation in Star and Linear Matrixes. Figure 1 shows the G' and G'' data of the blends of L329 probe in the star matrices at 40 °C (unfilled circles). The volume fraction of the probe is $v_{probe} = 0.01$. The filled circles and dotted curves indicate the behavior of the L329 probe and star matrices in their respective monodisperse states. For comparison, Figure 2 shows representative G' and G'' data obtained previously for the blends containing the same probe ($v_{probe} = 0.01$) in linear PI matrices.[19] As seen in Figures 1 and 2, the blends clearly exhibit fast and slow relaxation processes. The fast process is attributed to the terminal relaxation of the matrix and the partial relaxation of the high-M probe, and the slow process is assigned as the terminal relaxation of the probe, as noted for similar blends.[10,16−19] The terminal relaxation of the probe is retarded on an increase of the matrix molecular weight M_{mat}, which is indicative of the constraint release (CR) effect of the matrix on the probe relaxation that becomes less significant on the increase of M_{mat}. This retardation of the probe relaxation with M_{mat} is less significant than the retardation of the matrix relaxation itself, which is partly attributable to competition of CR and other mechanism (such as reptation) in the relaxation process of the linear L329 probe.

As seen in Figures 1 and 2, the complex modulus of the blends is close to that of respective matrices at angular frequencies ω above the terminal relaxation frequency of the matrices. This result, commonly seen for blends containing dilute probes,[3,10,16−19] indicates that the dilute probe chains negligibly affect the relaxation behavior of the matrix chains. Thus, the complex modulus of the matrix in the blend agrees with the modulus in its pure (monodisperse) state, $G_{mat}^*(\omega)$, except a difference in the matrix volume fraction (=$1 - v_{probe}$), and the modulus of the probe in the blend, $G_{probe}^*(\omega)$, is
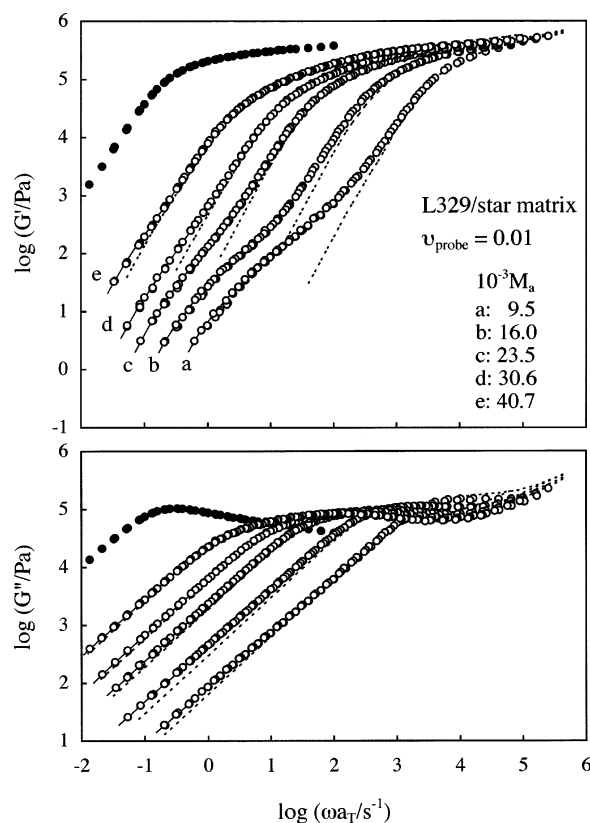

Figure 1. Storage and loss moduli, G' and G'', obtained for blends of the dilute linear PI probe (L329) in six-arm star PI matrices as indicated (unfilled circles). The data, obtained in this study, are reduced at 40 °C. The filled circles and dotted curves represent the moduli of the linear probe and star matrices in respective monodisperse systems.

evaluated from the $G_B^*(\omega)$ and $G_{mat}^*(\omega)$ data of the blend and pure matrix as[9,10,16−19]

$$G_{probe}^*(\omega) = G_B^*(\omega) - (1 - v_{probe})G_{mat}^*(\omega) \qquad (4)$$

In this paper, the previously utilized subscript[9,10,16−19] "1" and "2" are replaced by "mat" and "probe" (cf. eq 4) and the second subscripts indicating the state (in the blend or pure state) are omitted for clarity/simplicity of notation. (Since this paper examines only the blends containing dilute probes, no confusion would arise from this change in the notation.)

The relaxation behavior of the probe in the blend is most clearly examined for its storage modulus $G'_{probe}(\omega)$ evaluated with eq 4. This $G'_{probe}(\omega)$ is very close to $G'_B(\omega)$ of the blend at low ω where the matrix has fully relaxed (unless the matrix molecular weight is high and the low-ω shoulder of $G'_B(\omega)$ is not clearly resolved).

Figure 3 compares the $G'_{probe}(\omega)$ data of the L329 probe having different volume fractions $v_{probe} = 0.005$ and 0.01 in the same 6(I-16) star matrix. The reduced modulus $v_{probe}^{-1}G'_{probe}(\omega)$ for these v_{probe} values are indistinguishable and thus individual probe chains relax in the same way at $v_{probe} = 0.005$ and 0.01, confirming that the L329 probe is dilute and entangled only with the matrix chains in the range of $v_{probe} \leq 0.01$. (Note that the reduced molecular weight of the probe, $v_{probe}^{1.3}M_{probe} = 0.83 \times 10^3$ for $v_{probe} = 0.01$, is well below the entanglement spacing for PI, $M_e = 5.0 \times 10^3$.) In the remaining part of this paper, we focus on the relaxation behavior of the dilute L329 probe with $v_{probe} = 0.01$ in the star and linear matrices (Figures 1 and 2) to examine the constraint release process in the star matrices.

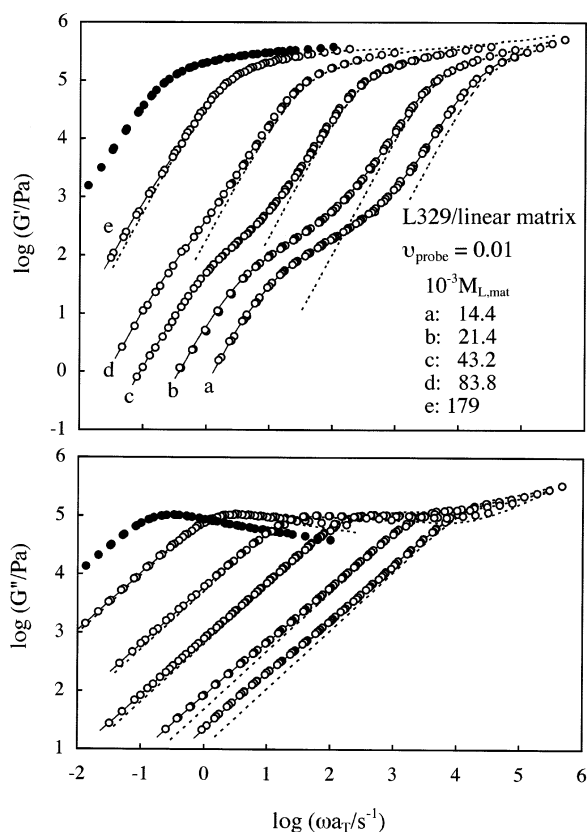**Figure 2.** Storage and loss moduli, G' and G'', obtained for blends of the dilute linear PI probe (L329) in linear PI matrices as indicated (unfilled circles). The data, obtained in the previous study,[19] are reduced at 40 °C. The filled circles and dotted curves represent the moduli of the linear probe and star matrices in respective monodisperse systems.
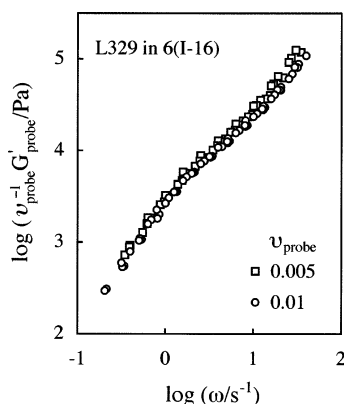

Figure 3. Comparison of the reduced storage modulus $v_{\text{probe}}{}^{-1}G'_{\text{probe}}$ at 40 °C obtained for the L329 probe having different volume fractions $v_{\text{probe}} = 0.005$ and 0.01 in the same 6(I-16) star matrix.

4.2. Relaxation Mode Distribution of Probe. The viscoelastic relaxation mode distribution of the probe is most clearly reflected in the ω dependence of its storage modulus, $G'_{\text{probe}}(\omega)$ (cf. eq 4). In Figure 4a, this dependence is compared for the dilute L329 probe ($v_{\text{probe}} = 0.01$) in various star matrices as indicated. For the clearest comparison of the shape of the G'_{probe} curve representing the ω dependence, we have chosen the curve in the 6(I-09) star matrix (arm molecular weight M_a = 9.5 × 10³) as a reference and shifted the curves in the other matrices horizontally by a factor of λ so as to superpose the low-ω tails of these curves (where $G'_{\text{probe}} \propto \omega^2$) onto that of the reference curve. For comparison, Figure 4b shows the G'_{probe}
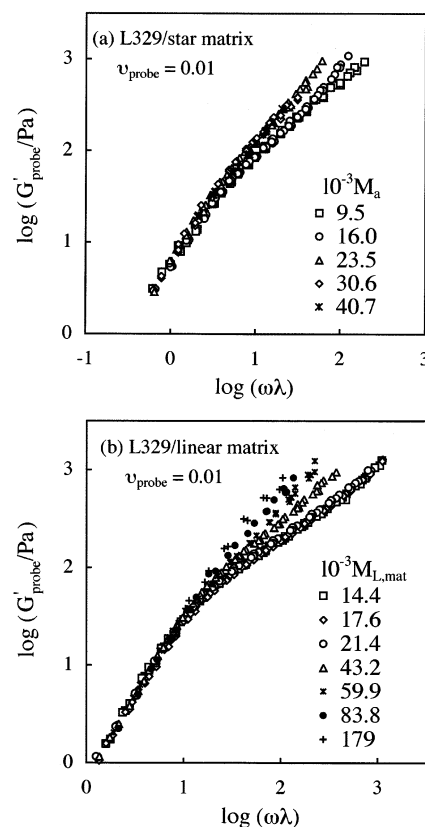

Figure 4. Comparison of the storage modulus (G'_{probe}) data at 40°C obtained for the L329 probe having $v_{\text{probe}} = 0.01$ in (a) various six-arm star PI matrices and (b) linear PI matrices. The data in the linear matrices were obtained in the previous study.[19] For the clearest comparison of the ω dependence of G'_{probe}, the G'_{probe} curve in the 6(I-09) star matrix with $M_a = 9.5 \times 10^3$ (for top panel) and/or in the L14 linear matrix with $M_{\text{L,mat}} = 14.4 \times 10^3$ (for bottom panel) was chosen as a reference and the curves in the other matrices were shifted horizontally by a factor of λ so as to superpose the low-ω tails of these curves (where $G'_{\text{probe}} \propto \omega^2$) onto that of the reference curve.

curve of the same probe (L329) in linear matrices obtained in the previous study.[19] These curves are shifted similarly, with the curve in a linear matrix of $M_{\text{L,mat}} = 14.4 \times 10^3$ being utilized as the reference.

As seen in Figures 4a and 4b, the G'_{probe} curve of the L329 probe becomes steeper with increasing M_a and/or $M_{\text{L,mat}}$ of the matrix. This change in the shape of the curve indicates that the slow relaxation mode distribution of the L329 probe becomes narrower and its terminal relaxation intensity increases on an increase of M_a and/or $M_{\text{L,mat}}$ above a threshold value, $M_{\text{L}}^{\text{th}} = 16.0 \times 10^3$ and $M_{\text{L,mat}}^{\text{th}} = 43.2 \times 10^3$. Note that these threshold values are much smaller than M_{probe} of the L329 probe.

The above changes of the relaxation mode distribution/intensity of the linear L329 probe chain are attributed to competition of its own reptation and constraint release (CR), the latter being activated by the matrix chain motion.[2,16,17,19] This competition is overwhelmed by the CR mechanism and the pure CR relaxation of the probe is observed only in the range of $M_a < M_a^{\text{th}}$ ($\ll M_{\text{probe}}$) and/or $M_{\text{L,mat}} < M_{\text{L,mat}}^{\text{th}}$ ($\ll M_{\text{probe}}$) where the matrix relaxes much faster than the probe therein. In this range, the relaxation mode distribution (CR mode distribution) of the probe does not change with the matrix molecular weight, as seen in Figure 4, parts a and b. This CR mode distribution can be most clearly examined for a normalized storage modulus defined by[3,9,19]

$$\tilde{G}'_{\text{probe}} \equiv \frac{M_{\text{probe}}}{\rho v_{\text{probe}} RT} G'_{\text{probe}} \qquad (5)$$

Here, ρ is the density of the system (blend), R is the gas constant, and T is the absolute temperature. In Figure 5, the normalized moduli of the L329 probe in the star and/or linear matrices having $M_a < M_a^{\text{th}}$ and/or $M_{\text{L,mat}} < M_{\text{L,mat}}^{\text{th}}$ are plotted against a normalized frequency $\omega\tau_{\text{probe}}$, where τ_{probe} is the experimentally determined probe relaxation time (more accurately, the second moment average relaxation time) explained later for Figure 6. The star matrix ($M_{\text{mat}} = 54.2 \times 10^3$; large unfilled circles) has the arm molecular weight $M_a = 9.5 \times 10^3 \ll M_{\text{probe}}$. For comparison, Figure 5 also shows the previous data[19] for various linear probes ($10^{-3} M_{\text{probe}} = 179$, 248, and 626) exhibiting the CR relaxation in much shorter linear matrices. For clarity of the plots, only representative data are shown.

In Figure 5, we first note that the normalized plots for the linear probes of various M_{probe} in the CR regime collapse into a universal curve. This fact indicates that the probes have the universal CR mode distribution in the normalized format. Furthermore, the $\tilde{G}'_{\text{probe}}$ data are quantitatively close to the solid curve that represents $\tilde{G}'_{\text{probe}}$ expected for the Rouse−CR mechanism,[2−4]

$$\tilde{G}'_{\text{probe}} = \sum_{p=1}^{N_{\text{probe}}} \frac{\omega^2 (15\tau_{\text{probe}}/\pi^2)^2 p^{-4}}{1 + \omega^2 (15\tau_{\text{probe}}/\pi^2)^2 p^{-4}} \quad \text{(for Rouse−CR)} \quad (6)$$

Here, the factor of $15\tau_{\text{probe}}/\pi^2$ (with τ_{probe} being the second moment average) is the longest relaxation time of the CR process of the probe.[19]

The above results clearly indicate that the terminal viscoelastic CR relaxation of the linear PI probe can be described by the Rouse−CR mechanism, as similar to linear polystyrene (PS) probes in linear/star PS matrices.[2,9,16,17] Thus, we can utilize, as a good approximation, the Rouse−CR expression of the CR time in our later analysis of the CR relaxation in star PI matrices (although delicate non-Rouse features have been also noted for the dielectrically determined eigenfunctions for the CR motion[2,20,28]).

In relation to this Rouse−CR feature of the probe, it should be noted that the dilute linear PI probes exhibited the purely CR relaxation behavior in linear matrices in a range of the Struglinski−Graessley[29] parameter, $r_{\text{SG}} \equiv M_{\text{probe}} M_e^{\ 2} M_{\text{L,mat}}^{-3} \geq 0.2$.[19] This range of r_{SG}, specifying the M_{probe} and $M_{\text{L,mat}}$ values of linear PI probes and matrices that allow the probe to exhibit pure CR behavior, is wider compared to that for linear/linear polystyrene blends,[3] $r_{\text{SG}} \geq 0.5$. Namely, the CR behavior can be more easily observed for PI. This result indicates that the probe relaxation is not uniquely determined by the entanglement numbers for the probe and matrix, $N_{\text{probe}} = M_{\text{probe}}/M_e$ and $N_{\text{L,mat}} = M_{\text{L,mat}}/M_e$, but is affected by additional molecular parameters such as the local CR gate number suggested by Graessley,[2] as discussed in the previous work.[19]

4.3. Relaxation Time of Linear L329 Probe. On the basis of eq 4, the terminal relaxation time of the probe in the blend is unequivocally evaluated from the G_B^* and G_{mat}^* data of the blend and pure matrix at low ω as

$$\tau_{\text{probe}} \equiv \left[\frac{G'_{\text{probe}}}{\omega G''_{\text{probe}}} \right]_{\omega \to 0} = \left[\frac{G'_B - (1 - v_{\text{probe}})G'_{\text{mat}}}{\omega \{ G''_B - (1 - v_{\text{probe}})G''_{\text{mat}} \}} \right]_{\omega \to 0} \quad (7)$$

This τ_{probe} is identical to the second moment average relaxation
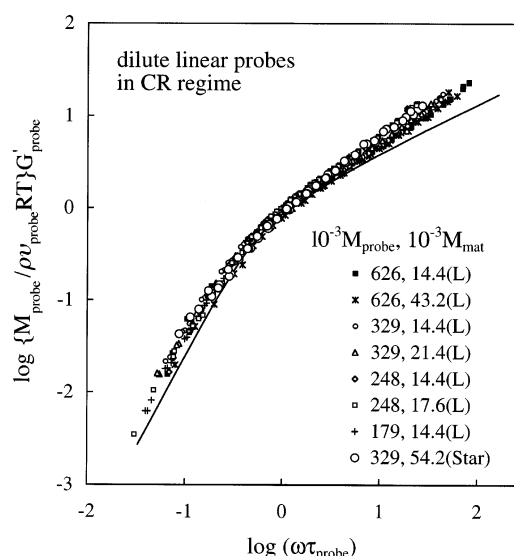

Figure 5. Normalized moduli $\{M_{\text{probe}}/\rho v_{\text{probe}} RT\}G'_{\text{probe}}$ of dilute linear PI probes in linear/star PI matrices much shorter than the probe (*in CR regime*). The data for the L329 probe in the 6(I-09) star matrix ($M_{\text{mat}} = 54.2 \times 10^3$; large unfilled circles) were measured in this study, and all other data (in the linear matrices) were obtained previously.[19] For the clearest examination of the viscoelastic CR mode distribution, the moduli data are plotted against a normalized frequency $\omega\tau_{\text{probe}}$, where τ_{probe} is the experimentally determined terminal relaxation time of the probe. (The τ_{probe} data for the L329 probe are summarized in Figure 6, and those for the other probes were documented in ref 19.) The solid curve indicates the prediction of the Rouse−CR model for linear probes (eq 6).
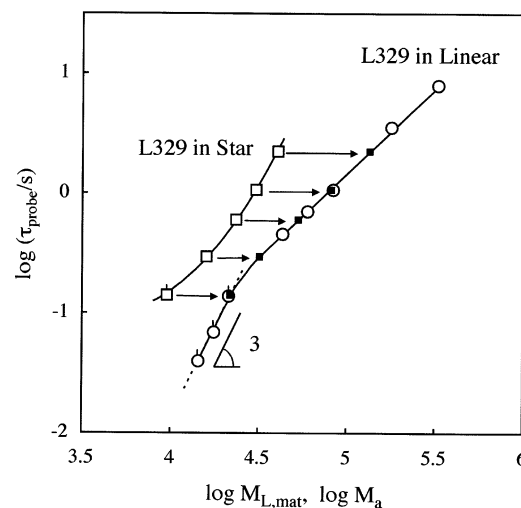

Figure 6. Plots of the terminal viscoelastic relaxation time (second moment average relaxation time) τ_{probe} of the dilute L329 probe in six-arm star PI matrices (large unfilled squares) and/or linear PI matrices (circles) at 40 °C. The symbols with pip indicate that the probe exhibited pure CR behavior in the given matrices. The τ_{probe} data in the star and linear matrices were obtained in this and previous[19] studies, respectively. These data are plotted against the molecular weight of the arm (for the star matrices) and/or the matrix chain as a whole (for the linear matrices). The small filled squares specify linear matrices that provide the probe with the relaxation environment equivalent to the environment in respective star matrices. For further details, see text.

time $\langle \tau \rangle$ defined in terms of the relaxation spectrum $H_{\text{probe}}(\tau)$ of the probe in the blend,[3,9,10,16−19] $\langle \tau \rangle = [\int_{-\infty}^{\infty} \tau^2 H_{\text{probe}} \, d(\ln \tau)] \times [\int_{-\infty}^{\infty} \tau H_{\text{probe}} \, d(\ln \tau)]^{-1}$. This average heavily weighs on slow relaxation modes, and thus τ_{probe} is close to the longest relaxation time.

In Figure 6, the τ_{probe} data of the dilute linear L329 probe in the star matrices are plotted against the molecular weight M_a

of the star arm (large unfilled squares). For comparison, the data of the same probe in linear matrices examined in the previous work[19] are plotted against the matrix molecular weight $M_{L,mat}$ (large unfilled circles). The data point for the highest $M_{L,mat}$ (=329×10^3) represents the relaxation time of the L329 probe in its monodisperse state. The small filled squares indicate $M_{L,mat}$ of linear matrices equivalent to respective star matrices, as explained later in more details.

In Figure 6, we first note that the M_a dependence of τ_{probe} in the star matrices becomes stronger with increasing M_a while the $M_{L,mat}$ dependence in the linear matrices becomes weaker with increasing $M_{L,mat}$. This difference can be partly related to the difference in the global motion of the matrix chains that activates the local CR process of the probe: The matrix relaxation time τ_{mat} (=product of the matrix viscosity η_{mat} and compliance J_{mat}) corresponding to this motion exhibits the exponential M_a dependence for the star matrices and the $M_{L,mat}^{3.5}$ power-law dependence for the linear matrices.

In fact, the above difference of τ_{probe} in the star and linear matrices is considerably diminished when τ_{probe} is plotted against τ_{mat} and/or η_{mat}, as shown in Figures 7a and 7b. At the same time, it should be also emphasized that the τ_{probe} data are never proportional to τ_{mat} and/or η_{mat} even in the CR regime where the probe exhibits the universal relaxation mode distribution. (The lack of the proportionality to η_{mat} indicates lack of the Stokes−Einstein behavior.) This fact is also noted in Figure 6 where τ_{probe} in the linear matrices in the CR regime (shown with the circles with pips) is proportional to $M_{L,mat}^3$, not to $M_{L,mat}^{3.5}$ as observed for τ_{mat}. Similarly, the M_a dependence of τ_{probe} in the star matrices is weaker than that of τ_{mat}. These differences of the M_{mat} dependencies of τ_{probe} and τ_{mat} can be related to the number of matrix chains penetrating/sustaining each entanglement point, as discussed previously.[3,19]

In relation to the above results, it should be emphasized that the power-law type $M_{L,mat}$ dependence of τ_{probe} in the linear matrices is observed only in a narrow range of $M_{L,mat}$ (circles with pips in Figure 6) where the probe exhibits the universal CR mode distribution (cf. Figure 5). This range is specified by $r_{SG} \equiv M_{probe}M_e^2M_{L,mat}^{-3} \geq 0.2$.[19] The $M_{L,mat}$ dependence weakens on an increase of $M_{L,mat}$ beyond this range and this weakening, associated with the change in the mode distribution (cf. Figure 4b), is attributed to the competition of the CR and reptation mechanisms in the probe relaxation.

For convenience of later analysis, we here summarize the $M_{L,mat}$ and M_{probe} dependencies of the terminal (second-moment average) CR relaxation time τ_{linear}^{CR} of linear probes in linear matrices. In the range of $r_{SG} \geq 0.2$ (CR regime), τ_{linear}^{CR} is proportional to $M_{L,mat}^3$ (cf. circles with pip in Figure 6) and to M_{probe}^2, as shown in the previous work.[19] Figure 8 summarizes these τ_{linear}^{CR} data for various linear probes (having $10^{-3} M_{probe}$ = 179−626) obtained in the previous work.[19] The data, plotted against $M_{L,mat}^3M_{probe}^2$, are well described by an empirical equation shown with the solid curve,

$$\tau_{linear}^{CR} = 10^{-25.0}M_{L,mat}{}^3M_{probe}{}^2 = 2.5 \times 10^{-18}M_{L,mat}{}^3N_{probe}{}^2$$
$$\text{(in s) in linear PI matrices at 40 °C} \quad (8)$$

This empirical equation is later utilized in our evaluation of the CR time of the star matrices. (The τ_{linear}^{CR} data in the linear matrices were equally well described by an empirical equation with a little smaller $M_{L,mat}$ exponent, $\tau_{linear}^{CR} = 10^{-24.15}M_{L,mat}{}^{2.8}M_{probe}{}^2$ (in s), as shown from an extensive test of the τ^{CR} data in the previous study.[19] However, the CR time
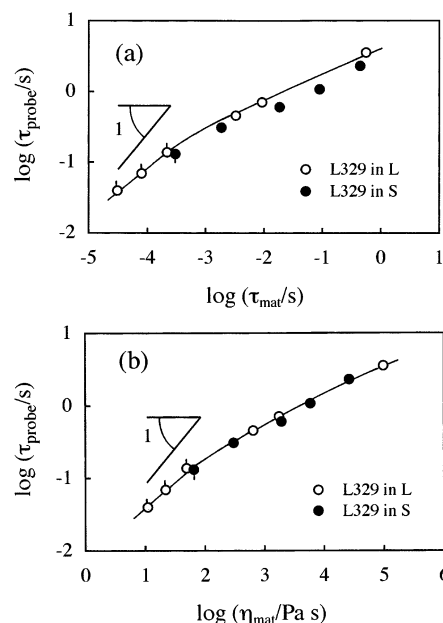

Figure 7. Plots of the terminal relaxation time τ_{probe} of the dilute L329 probe at 40 °C against (a) star/linear matrix relaxation time and (b) matrix viscosity. The symbols with pip indicate that the probe exhibited pure CR behavior in the given matrices.
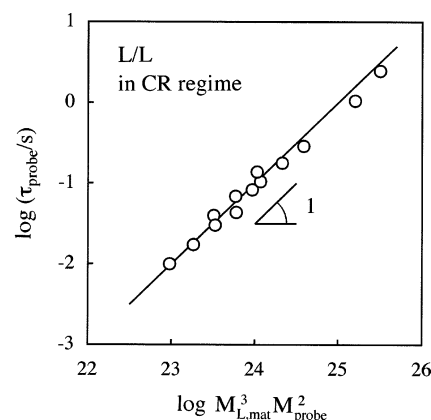

Figure 8. Terminal viscoelastic relaxation time τ_{probe} of various dilute linear PI probes in much shorter linear matrices (*in CR regime*). The τ_{probe} data at 40 °C, obtained in the previous studies,[19,22] are plotted against $M_{L,mat}^3M_{probe}^2$. The solid line indicates the empirical eq 8.

of the star matrices evaluated with this equation was practically indistinguishable from that with eq 8.)

4.4. CR Relaxation Time of Monodisperse Star PI. As explained earlier, the CR relaxation time τ_{star}^{CR} of the star matrix can be evaluated from the molecular weight $M_{L,mat}$* of the linear matrix that has an *equivalent* effect on the probe relaxation. Now, we apply this method to the data summarized in Figure 6 to evaluate τ_{star}^{CR} for our moderately entangled star PI matrices. The $M_{L,mat}$* values are specified in Figure 6 with the small filled squares, and the entanglement lifetime $\tau_{life}(star)$ in the given star matrix is evaluated from this $M_{L,mat}$* value with the aid of eqs 1 and 8 as

$$\tau_{life}(star) = 2.5 \times 10^{-18}\{M_{L,mat}*\}^3 \text{ (in s)} \quad (9)$$

Substituting this $\tau_{life}(star)$ value in eq 3, we obtained the CR time τ_{star}^{CR} of our moderately entangled star PI matrices in their monodisperse state.

Figure 9a compares this τ_{star}^{CR} (small filled squares) with the observed relaxation time τ_{star}^{obs} of these star PI systems (unfilled
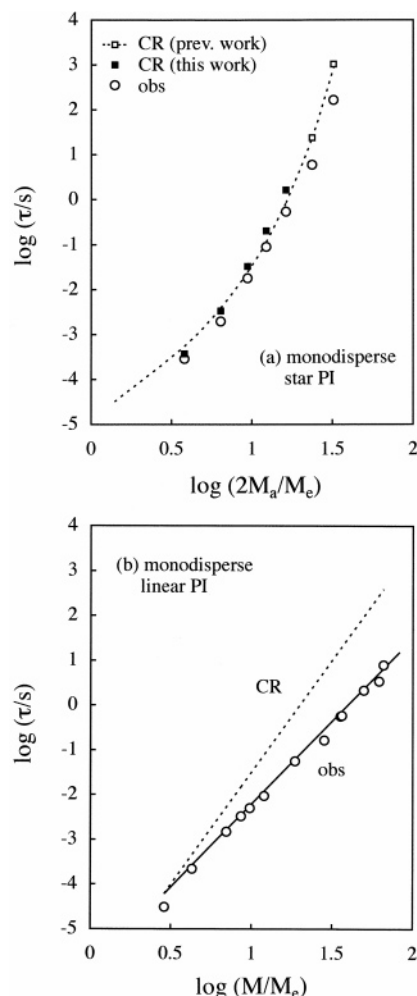
Figure 9. Comparison the viscoelastic CR relaxation time τ^{CR} for monodisperse systems of star and linear PI chains with the observed terminal relaxation time τ^{obs} (circles) at 40 °C. For the star PI system (top panel), unfilled and filled squares indicate τ^{CR}_{star} obtained from viscoelastic data of star/star[19] and linear/star blends, respectively, and the dotted curves denote τ^{CR}_{star} evaluated with the previously reported empirical equation,[19] $\tau^{CR}_{star} = 4.0 \times 10^{-5} N_a^2 \exp\{0.71\ N_a\}$ (in s). For the linear PI systems (bottom panel), τ^{CR}_{linear} was evaluated from the empirical eq 8.

circles). These τ^{CR}_{star} and τ^{obs}_{star} data are plotted against the number of entanglements per span length, $2M_a/M_e$. Small unfilled squares show the τ^{CR}_{star} data of highly entangled (high-M_a) star PI obtained previously with the standard method,[18] the evaluation of τ^{CR}_{star} from the star PI/star PI blend moduli, and the dotted curve indicates an empirical equation of τ^{CR}_{star} obtained from these τ^{CR}_{star} data for the high-M_a stars ($\tau^{CR}_{star}/s = 4.0 \times 10^{-5} N_a^2 \exp\{0.71 N_a\}$).[18] The τ^{CR}_{star} data obtained with the current method (small filled squares) are in satisfactory agreement with this empirical equation, lending support to the validity of this method.

More importantly, Figure 9a demonstrates that τ^{CR}_{star} is not very longer than τ^{obs}_{star} for the monodisperse star PI in a considerably wide range of M_a/M_e between 2 and 16. This fact, most clearly noted for the $\tau^{CR}_{star}/\tau^{obs}_{star}$ ratio (circles) shown in Figure 10, suggests that the CR mechanism significantly contributes to the actual relaxation of the star PI in this range of M_a/M_e. This conclusion is consistent with the validity of the molecular picture of partial dynamic-tube-dilation (p-DTD) discussed later for Figure 11.
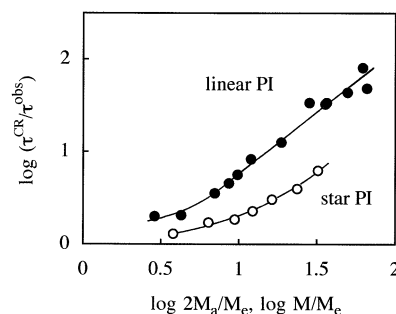

Figure 10. Comparison of τ^{CR}/τ^{obs} ratios for monodisperse star and linear PI systems at 40 °C. (The τ^{CR} and τ^{obs} data are summarized in Figure 9.)
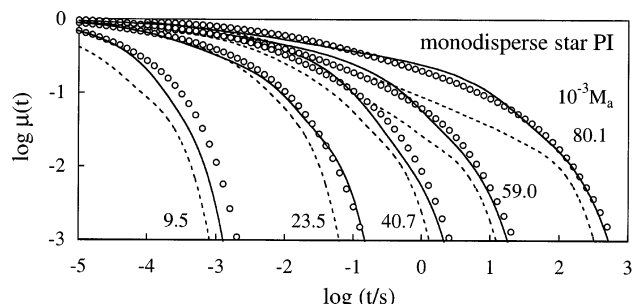

Figure 11. Comparison of the normalized relaxation modulus μ (circles) of monodisperse star PI systems at 40 °C with μ_{p-DTD} (solid curves) and μ_{f-DTD} (dotted curves) expected for the partial- and full-DTD processes. The μ_{f-DTD} was obtained from the dielectric data under the full-DTD assumption, while μ_{p-DTD} was evaluated from the dielectric data and τ^{CR}_{star} data (Figure 9) without this assumption. For further details, see text.

For monodisperse systems of linear PI examined in the previous study,[19] Figure 9b compares the CR time and observed relaxation time, τ^{CR}_{linear} (dotted line; eq 8 with $M_{L,mat} = M_{probe}$) and τ^{obs}_{linear} (circles), and Figure 10 shows the $\tau^{CR}_{linear}/\tau^{obs}_{linear}$ ratio (filled circles). Differing from the behavior of star PI, τ^{obs}_{linear} of linear PI is much smaller than τ^{CR}_{linear} in the well entangled regime. This result suggests that the CR mechanism has an only minor effect on the terminal relaxation time of well entangled linear chains, although the terminal relaxation mode distribution is considerably affected by this mechanism.[19] Thus, the CR mechanism plays a quite different role in the terminal relaxation of the star and linear chains. A related difference has been noted for blends containing nondilute probes that were entangled among themselves as well as with the matrices.[13]

4.5. Partial- and Full-DTD Pictures for Monodisperse Star PI. The CR mechanism undoubtedly allows the topological constraint (represented as a tube) to loosen with time, and this loosening gives a basis of the molecular picture of dynamic tube dilation (DTD). This picture is classified into the full-DTD and partial-DTD pictures, the former being based on an assumption that the relaxed portions of the chain do not effectively constrain the unrelaxed portion and behave as a simple solvent while the latter considering the magnitude of tube dilation to be determined by a balance of the full-DTD motion of the probe chain and a CR-displacement of this chain. These molecular pictures lead to different expressions of the normalized relaxation modulus $\mu(t) = G(t)/G_N$ (with G_N being the entanglement plateau modulus) of monodisperse star systems:[18]

$$\mu(t) = \varphi'(t)/\beta(t) \tag{10}$$

with

$$\beta_{\text{f−DTD}}(t) = \{\varphi'(t)\}^{-d} \quad \text{(with } d \cong 1.3 \text{ for PI}^{22}) \text{ for full-DTD}$$
(11a)

and

$$\beta_{\text{p−DTD}}(t) = \min[\beta_{\text{f−DTD}}(t); \quad \beta_{\text{CR}}(t)] \text{ for partial-DTD} \quad (11b)$$

Here, $\varphi'(t)$ is the survival fraction of the dilated tube that can be determined from dielectric data if the chain has type-A dipoles (which is the case for PI),[18,22,23,30] and $\beta_{\text{CR}}(t)$ is the maximum number of the entanglement segments that are mutually equilibrated with the CR mechanism in a given time scale of t. The dilation exponent d, experimentally determined from the low-ω plateau height of G' for linear/linear blends containing mutually entangled high-M components, is close to 1.3 for PI.[22,31] For the star probe, $\beta_{\text{CR}}(t)$ is evaluated from the terminal viscoelastic CR time $\tau_{\text{star}}^{\text{CR}}$ on the basis of the tethered-Rouse dynamics as[18]

$$\beta_{\text{CR}}(t) = N_{\text{a}} \left[\sum_{p=1}^{N_{\text{a}} - N_{\text{f}}} \exp\left(-\frac{r_p t}{2\tau_{\text{star}}^{\text{CR}}}\right) + \sum_{q=1}^{N_{\text{f}}} \exp\left(-\frac{r_q' t}{\tau_{\text{f}}}\right) \right]^{-1} \quad (12)$$

In eq 12, the factor of $2\tau_{\text{star}}^{\text{CR}}$ represents the terminal dielectric CR time, and τ_{f} and $N_{\text{f}} (\cong N_{\text{a}}^{1/2})$ are the longest relaxation time for the contour length fluctuation (CLF) of the star arm and the number of entanglement segments corresponding to the amplitude of CLF, respectively. The factor r_{p} appearing in eq 12 represents the tethered-Rouse type ratio of $\tau_{\text{star}}^{\text{CR}}$ to the characteristic time of the pth viscoelastic CR mode, and the factor r_q' is the ratio of τ_{f} to the relaxation time of qth CLF mode. For monodisperse star chains, r_p and r_q' are expressed as[18,32]

$$r_p = \sin^2\left(\frac{\pi\{2p-1\}}{2\{2N_{\text{a}}+1\}}\right) \sin^{-2}\left(\frac{\pi}{2\{2N_{\text{a}}+1\}}\right) \quad (13a)$$

and

$$r_q' = \sin^2\left(\frac{\pi\{2q-1\}}{2\{2N_{\text{f}}+1\}}\right) \sin^{-2}\left(\frac{\pi}{2\{2N_{\text{f}}+1\}}\right)$$
$$\text{with } N_{\text{f}} \cong N_{\text{a}}^{1/2} \quad (13b)$$

The r_{p} and r_q' values are obtained from the N_{a} value (cf. eq 13), and τ_{f} can be evaluated from the data for the dielectric relaxation time of linear PI[26,28] in the nonentangled regime: $\tau_{\text{f}}/\text{s} \cong 9.3 \times 10^{-13} M_{\text{a}}^2$ at 40°C.[18,33] Thus, β_{CR} (eq 12) is experimentally determined from the $\tau_{\text{star}}^{\text{CR}}$ data summarized in Figure 9.

In Figure 11, the $\mu(t)$ data of the star PI matrices in their monodisperse states (converted from the G^* data) are compared with the moduli for the full-DTD and partial-DTD processes, $\mu_{\text{f−DTD}}(t)$ (eqs 10 and 11a; dotted curves) and $\mu_{\text{p−DTD}}(t)$ (eqs 10 and 11b; solid curves), with the tube survival fraction $\varphi'(t)$ necessary for evaluation of $\mu_{\text{f−DTD}}(t)$ and $\mu_{\text{p−DTD}}(t)$ being evaluated from the dielectric data obtained in this and previous[24,25] studies. The μ data are much closer to $\mu_{\text{p−DTD}}$ than to $\mu_{\text{f−DTD}}$, indicating that the full-DTD picture fails severely but the partial-DTD picture works considerably well for the monodisperse star PI systems. This conclusion, being obtained for the high-M_{a} star PI in the previous study and confirmed for the moderately entangled stars in this study, indicates the importance of the CR mechanism in the terminal relaxation of the entangled star PI chains. (Similar behavior was noted for star polystyrenes.[10])

Finally, we should remember that the full-DTD picture works as a good approximation for monodisperse systems of *linear* PI.[26,28,34] Thus, this picture has a different validity for linear and star chains. This difference is related to the full-DTD diameter $a_{\text{f−DTD}}$ of the tube:[22,23,26] For the monodisperse linear chains having a narrow distribution of the relaxation modes, $a_{\text{f−DTD}}$ remains rather small even in the terminal regime and thus the segments within $a_{\text{f−DTD}}$ can be CR-equilibrated in time. In contrast, for the monodisperse star chains having a broad mode distribution, $a_{\text{f−DTD}}$ becomes considerably large in the terminal regime and the CR-equilibration over $a_{\text{f−DTD}}$ cannot occur in time thereby leading to the failure of the full-DTD picture. Thus, the topological architecture of the chain has a large influence on the validity of this picture.

In relation to this influence, we expect that the partial-DTD picture works well also for complicatedly branched chains such as comb, pom-pom, and hyperbranched chains. In addition, the full-DTD picture may work better (but not necessarily well) for the arms of these complicatedly branched chains than for the arms of the simple star chains because the trunks in the former class of chains would not relax prior to the arms and thus suppress the increase of $a_{\text{f−DTD}}$. A test of these expectations is considered as an interesting subject of future work.[35]

5. Concluding Remarks

For the purpose of examining the constraint release (CR) contribution to relaxation of moderately entangled six-arm star PI, we conducted linear viscoelastic tests for blends of these star PI and dilute high molecular weight (M) linear PI, the latter behaving as a probe entangled only with the matrix star chains. The terminal relaxation of this dilute linear probe occurred through competition of reptation and Rouse-type constraint release (CR). The probe relaxation time τ_{probe} measured in the blends was utilized to evaluate the CR time $\tau_{\text{star}}^{\text{CR}}$ of the star matrices themselves with the aid of an empirical equation for the probe CR time in linear matrices. It turned out that this $\tau_{\text{star}}^{\text{CR}}$ was considerably close to the observed relaxation time of the star PI, which indicates that the CR mechanism has a significant contribution to the terminal relaxation of stars in a wide range of $M_{\text{a}}/M_{\text{e}}$. Validity of the partial-DTD picture, found for the star PI systems in a wide range of $M_{\text{a}}/M_{\text{e}}$, was consistent with this significance of the CR mechanism. In addition, a difference from monodisperse linear PI systems (rather minor CR contribution to the terminal relaxation time of linear PI) suggests that the topological architecture of the chain has a large influence on the CR contribution.

References and Notes

(1) Doi, M.; Edwards, S. F. *The Theory of Polymer Dynamics*; Clarendon: Oxford, U.K., 1986.
(2) Graessley, W. W. *Adv. Polym. Sci.* **1982**, *47*, 67.
(3) Watanabe, H. *Prog. Polym. Sci.* **1999**, *24*, 1253.
(4) McLeish, T. C. B. *Adv. Phys.* **2002**, *51*, 1379.
(5) Archer, L. A.; Varshney, S. K. *Macromolecules* **1998**, *31*, 6348.
(6) Archer, L. A.; Juliani. *Macromolecules* **2004**, *37*, 1076.
(7) Simon, P. F. W.; Muller, A. H. E.; Pakula, T. *Macromolecules* **2001**, *34*, 1677.
(8) Kharchenko, S. B.; Kannan, R. M. *Macromolecules* **2003**, *36*, 407.
(9) Yoshida, H.; Watanabe, H.; Kotaka, T. *Macromolecules* **1991**, *24*, 572.
(10) Watanabe, H.; Yoshida, H.; Kotaka, T. *Macromolecules* **1992**, *25*, 2442.

(11) Milner, S. T.; McLeish, T. C. B.; Young, N. R.; Hakiki, A.; Johnson, J. M. *Macromolecules* **1998**, *31*, 9345.

(12) Blottiere, B.; McLeish, T. C. B.; Hakiki, A.; Young, R. N.; Milner, S. T. *Macromolecules* **1998**, *31*, 9295.

(13) Lee, J. H.; Fetters, L. J.; Archer, L. A.; Halasa, A. F. *Macromolecules* **2005**, *38*, 3917.

(14) Wang, S. F.; Wang, S. Q.; Halasa, A.; Hsu, W. L. *Macromolecules* **2003**, *36*, 5355.

(15) Park, S. J.; Larson, R. G. *J. Rheol.* **2006**, *50*, 21.

(16) Watanabe, H.; Sakamoto, T.; Kotaka, T. *Macromolecules* **1985**, *18*, 1436.

(17) Watanabe, H.; Kotaka, T. *Macromolecules* **1986**, *19*, 2520.

(18) Watanabe, H.; Sawada, T.; Matsumiya, Y. *Macromolecules* **2006**, *39*, 2553.

(19) Sawada, T.; Qiao, X.; Watanabe, H. *Nihon Reoroji Gakkaishi* (*J. Soc. Rheol. Jpn.*) **2006**, in press.

(20) Matsumiya, Y.; Watanabe, H.; Osaki, K.; Yao, M.-L. *Macromolecules* **1998**, *31*, 7528.

(21) Watanabe, H.; Matsumiya, Y.; Osaki, K.; Yao, M.-L. *Macromolecules* **1998**, *31*, 7538.

(22) Watanabe, H.; Ishida, S.; Matsumiya, Y.; Inoue, T. *Macromolecules* **2004**, *37*, 1937.

(23) Watanabe, H.; Ishida, S.; Matsumiya, Y.; Inoue, T. *Macromolecules* **2004**, *37*, 6619.

(24) Yoshida, H.; Adachi, K.; Watanabe, H.; Kotaka, T. *Polym. J.* **1989**, *21*, 863.

(25) Watanabe, H.; Matsumiya, Y.; Osaki, K. *J. Polym. Sci., Part B: Polym. Phys.* **2000**, *38*, 1024.

(26) Watanabe, H.; Matsumiya, Y.; Inoue, T. *Macromolecules* **2002**, *35*, 2339.

(27) Ferry, J. D. *Viscoelastic Properties of Polymers*, 3rd ed.; Wiley: New York, 1980.

(28) Watanabe, H. *Macromol. Rapid Commun.* **2001**, *22*, 127.

(29) Struglinski, M. J.; Graessley, W. W. *Macromolecules* **1985**, *18*, 2630.

(30) In Appendix of ref 18, $\beta_{f-DTD}(t) = \{\varphi'(t)\}^{-d}$ was mistyped as $\beta_{f-DTD}(t) = \{\varphi'(t)\}^{-d/2}$.

(31) The dilution exponent d changes a little with the chemical structure of the chain: $d \cong 1.3$ for PI and $d \cong 1$ for PS, as explained previously.[22] A molecular origin of this change deserves a further study.

(32) The ratio r'_q given by eq 13b is approximate because it is formulated for a portion of the probe composed of only N_f entanglement segments.[18]

(33) This τ_f was obtained by applying a relationship between the Rouse fluctuation times of tethered and free linear chains of the same M, $\tau_f^{tethered}(M) = 4\tau_f^{free}(M)$, to the data for the dielectric relaxation time of nonentangled linear PI.[26,28]

(34) Matsumiya, Y.; Watanabe, H.; Osaki, K. *Macromolecules* **2000**, *33*, 499.

(35) The test of the full- and partial-DTD pictures for complicatedly branched chains can be achieved through comparison of viscoelastic and dielectric data. In relation to this point, we should remember that the molecular model based on the full-DTD picture can reproduce the viscoelastic data of star chains but fails to describe the viscoelastic and dielectric data in a consistent way.[18,26] This fact indicates that a comparison of the viscoelastic data and predictions of the full-DTD molecular model(s) is not sufficient for the test of the full-DTD picture.